Preprints of the 21st IFAC World Congress (Virtual)
Berlin, Germany, July 12-17, 2020

Double-Hidden-Layer Recurrent Neural Network Fractional-Order Sliding Mode Control of Shunt Active Power Filter

Juntao Fei, Huan Wang, Mingang Hua

College of IoT Engineering, Hohai University, Changzhou, 213022 , China
(Tel: 86-519-85192023; e-mail: jtfei@hhu.edu.cn).

Abstract: In this paper, a fractional-order sliding mode control scheme based on a double-hidden-layer recurrent neural network is proposed for a single-phase shunt active power filter. Considering the shortcomings of traditional neural networks that the approximation accuracy is not high and weight and center vector of neural networks are unchangeable, a new double-hidden-layer recurrent neural network structure which contains two hidden layers to make the network have more powerful fitting ability, is designed to approximate the unknown nonlinearities. An original output feedback neural network with two hidden layers is designed to estimate the uncertainties regardless of unknown system characteristics and external disturbances. A fractional-order term is added to the sliding mode controller to have more adjustable space and better optimization space. Experimental results verified the validity of the designed controller and proved that it can complete the current compensation well with acceptable current tracking error, demonstrating the outstanding compensation performance and strong robustness

Keywords: Fractional-order control, Sliding mode control, Recurrent neural network (RNN), Double-hidden-layer recurrent neural network (DHLRNN).

1. INTRODUCTION

The rapid development of power electronics technology has made serious problems of harmonic pollution of power grids. Compared with various harmonic compensation methods, active power filters (APF) has strong real-time tracking performance, compensation capability, and good harmonic suppression. APF is one of the most important means to solve the harmonic problem in the power grid.

At present, APF control strategies mainly include hysteresis control, single-cycle control, triangular wave control and sliding mode control. Sliding mode control method (SMC), which is robust to external disturbances and parameter uncertainties, is widely used in nonlinear systems. An adaptive SMC method was proposed to make the tracking error converge to a small neighbourhood (Liu et al. 2019). A high-order sliding mode observer was applied for uncertain pure-feedback nonlinear systems (Park et al. 2019). An integral SMC method was studied for nonlinear systems with input disturbances (Fan et al. 2016). A new sliding mode fault-tolerant control method was designed for uncertain linear systems (Hao et al. 2017). A terminal sliding-mode-based cooperative control method was proposed for nonlinear systems (Chen et al. 2018).

The ordinary sliding surface is mainly composed of the error of system state or the integer-order calculus of the error. With the development of fractional calculus, the researchers begin to study the application of the fractional-order in SMC. Fractional-order was introduced to represent changes of the desired trajectory (Ionescu et al. 2015). Fractional-order differential technique was for crawler cranes (Tuan. 2019). A fractional-order adaptive control method was proposed for fuzzy singularly perturbed systems (Song et al. 2019).

Although the fractional-order sliding mode controller can obtain good tracking performance, however, the controller can be realized only if the system structure is fully understood, which is difficult to achieve in real life. In nonlinear systems, there are often some unknown nonlinear functions. Neural network (NN) is widely used in nonlinear system due to its universal approximation, which means it can approximate any unknown smooth nonlinear function. NN was used to approximate the nonlinear part in the active power filter (Fang et al. 2019). In recent research, many scholars have changed the structure of neural networks to improve the approximation accuracy, such as increasing feedback items or the number of hidden layers. A double-hidden-layer neural network was designed for a class of dynamic systems (Chu et al. 2019). A recurrent neural network was proposed to approximate the nonlinear part of the system (Wang et al. 2019).

Motivated by the above studies and researches, this paper proposes a fractional-order sliding mode controller based on double-hidden-layer recurrent neural network (DHLRNN) for the current control of an APF. Recurrent layers added in the input layer and the first hidden layer store more information and have better approximation effect. The main contribution can be summarized as:

(1) A new double-hidden-layer recurrent neural network with multiple computational layers, which can approximate any continuous function with arbitrary precision, is designed to approximate the unknown nonlinear part of APF. Compared with the single-hidden-layer neural network, the double-hidden-layer recurrent neural network is a deep neural

network, which can achieve a high precision approximation with fewer nodes.

(2) At the same time, the output feedback is introduced in the first hidden layer and the outer layer of the double hidden layer neural network to store more information, which can achieve better approximation effect. The proposed DHLRNN can realize the self-adjustment of the base width, center vector, weight and hidden layer feedback weight in spite of the initial values under the action of the adaptive law.

(3)A fractional-order term is added to the sliding mode controller. Compared with the intermittent adjustment of the integer-order sliding mode controller, the fractional-order sliding mode controller has more adjustable space and better optimization space. Fractional sliding mode controller combines the advantages of fractional calculus and sliding mode control, improving the control precision and performance.

2. DYNAMICS OF ACTIVE POWER FILTER

Fig.1 is the basic circuit structure of a single-phase active power filter. In Fig.1, v_s is a grid voltage, i_s is a grid current, i_c is a filter output compensation current, L is an AC inductor, R is an equivalent resistor, C is the DC capacitor.

According to the circuit theory and Kirchhoff's voltage law, the following equation can be derived as:

$$v_S = L\frac{di_c}{dt} + Ri_c + u_{MN} \tag{1}$$

where $u_{MN} = u \cdot u_c$, u is a switch function satisfying that $\mathrm{u} = \begin{cases} 1 & \text{if } S_2, S_3 \text{ are on, and } S_1, S_4 \text{ are off} \\ -1 & \text{if } S_1, S_4 \text{ are on, and } S_2, S_3 \text{ are off} \end{cases}$.

Then we can get:

$$\frac{di_c}{dt} = -\frac{R}{L}i_c + \frac{v_s}{L} - \frac{v_{dc}}{L}u \tag{2}$$

The derivative of equation (2) becomes:

$$\frac{d^2i_c}{dt^2} = \frac{R^2}{L^2}i_c - \frac{Rv_s}{L^2} + (\frac{R}{L^2}v_{dc} - \frac{1}{L}\frac{dv_{dc}}{dt})u \tag{3}$$

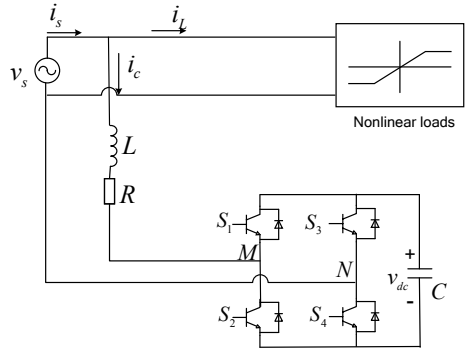

Fig.1. Schematic structure of single-phase active power filter

In the actual operation process, APF will be affected by various unknown disturbances, and the aging of the grid side inductor and DC side capacitor will cause parameter perturbation. In order to improve the robustness in the presence of external disturbances and parameter perturbations, it is necessary to consider the above effects in the system model. Assuming that the lumped unknown disturbance is F, then the mathematical model of APF can be expressed as:

$$\frac{d^2i_c}{dt^2} = \frac{R^2}{L^2}i_c - \frac{Rv_s}{L^2} + (\frac{R}{L^2}v_{dc} - \frac{1}{L}\frac{dv_{dc}}{dt})u + F \tag{4}$$

Define $x = i_c$, and the system can be simplified as the following equation.

$$\frac{d^2x}{dt^2} = f(x) + bu + F \tag{5}$$

where $f(x)$ is $\frac{R^2}{L^2}i_c - \frac{Rv_s}{L^2}$, $b = \frac{R}{L^2}v_{dc} - \frac{1}{L}\frac{dv_{dc}}{dt}$, and F is the lumped disturbance, which contains parameter uncertainties and external disturbance. It is assumed that the upper bound of the lumped disturbance F is a positive constant F_d, satisfing $|F| \le F_d$.

3. FRACTIONAL-ORDER SLIDING MODE CONTROLLER

Fractional-order calculus is defined as:

$${}_aD_t^\alpha \begin{cases} \frac{d^\alpha}{dt^\alpha} & \alpha > 0 \\ 1 & \alpha = 0 \\ \int_a^t (d\tau)^\alpha & \alpha < 0 \end{cases} \tag{6}$$

where ${}_aD_t^\alpha$ is the symbol of the fractional-order calculus, a and t are the upper and lower bounds of the operation, α is the order of the fractional-order calculus.

We use the Caputo fractional-order for the proposed control method. Caputo fractional-order is defined as follows:

$$D^\alpha f(t) = \frac{1}{\Gamma(n-\alpha)}\int_0^t \frac{f^{(n)}(\tau)}{(t-\tau)^{\alpha-n+1}}d\tau, \quad n-1 < \alpha < n \tag{7}$$

where $\Gamma(\cdot)$ is a gamma function, n takes the value one.

Consider the APF model in equation (5), we define that reference current is x_d. The goal of the control system is to make the actual current track the reference current and make the tracking error $e = x - x_d$ as small as possible.

Define the first derivative of tracking error and the second derivative of tracking error are $\dot{e} = \dot{x} - \dot{x}_d$ and $\ddot{e} = \ddot{x} - \ddot{x}_d$.

Define the fractional-order sliding surface as:

$$s = \dot{e} + c_1 e + c_2 D^{\alpha-1}e \tag{8}$$

where c_1 and c_2 are the constant, $D^{\alpha-1}e$ is the $\alpha-1$ order derivative of the tracking error, and $0 < \alpha < 1$.

Making the derivative of the fractional sliding surface gets

$$\begin{aligned} \dot{s} &= \ddot{e} + c_1\dot{e} + c_2 D^\alpha e \\ &= \ddot{x} - \ddot{x}_d + c_1\dot{e} + c_2 D^\alpha e \\ &= f(x) + bu + F - \ddot{x}_d + c_1\dot{e} + c_2 D^\alpha e \end{aligned} \tag{9}$$

Without considering the lumped uncertainties, the equivalent control law can be obtained by making $\dot{s} = 0$.

$$u_{eq} = -\frac{1}{b}(f(x) - \ddot{x}_d + c_1\dot{e} + c_2 D^\alpha e) \tag{10}$$

Design the switching control law as:

$$u_{sw} = -K\,\mathrm{sgn}(s) \tag{11}$$

where K is a constant.

Then a comprehensive controller is proposed is

$$u = u_{eq} + u_{sw} = -\frac{1}{b}(f(x) - \ddot{x}_d + c_1\dot{e} + c_2 D^{\alpha} e) - K\,\mathrm{sgn}(s) \tag{12}$$

However, if $f(x)$ in (12) is unknown, it is impossible to implement the controller (12). A double-hidden-layer recurrent neural network approximator is proposed in next step to solve this problem.

4. DOUBLE-HIDDEN-LAYER RECURRENT NEURAL NETWORK (DHLRNN) FRACTIONAL-ORDER SLIDING MODE CONTROLLER (DHLRNNFSMC)

Fig.2 is a double-hidden-layer recurrent neural network structure that comprises four layers, namely an input layer, a first hidden layer, a second hidden layer and an output layer.

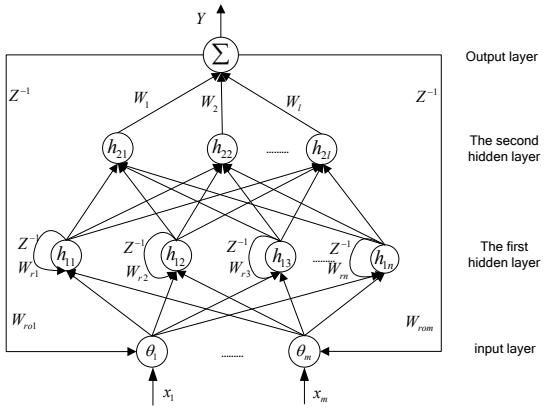

Fig.2.Double-hidden-layer recurrent neural network structure

The input layer of the double-hidden-layer recurrent neural network completes the transmission of the input signal, and receives the output signal exY of the feedback signals of the output layer. The output expression of the input layer is:

$$\theta_i = x_i \cdot W_{roi} \cdot exY \ , \ i = 1,2,...,m \tag{13}$$

The signal is mapped from the input layer space to the first hidden layer space, and a feedback loop is added into the first hidden layer to complete the signal feedback. $H_2 = [h_{21}, h_{22}, ..., h_{2l}]^T$ is Gaussian function, and the Gaussian function of the j-th node is calculated as:

$$h_{1j} = e^{-net_{1j}} \ , \ net_{1j} = \sum_{i=1}^{m} \frac{\left|\theta_i + W_{rj} exh - c_{1j}\right|^2}{b_{1j}^2} \ , \ k = 1,2,...,l \tag{14}$$

where c_{1j} is the center vector, and b_{1j} is the base width.

The second hidden layer maps the signal from the first hidden layer space to the second hidden layer space, and $H_1 = [h_{11}, h_{12}, ..., h_{1l}]^T$ is Gaussian function, and the Gaussian function of the k-th node is calculated as:

$$h_{2k} = e^{-net_{2k}} \ , \ net_{2k} = \sum_{i=1}^{n} \frac{\left|h_{1j} - c_{2k}\right|^2}{b_{2k}^2} \ , \ k = 1,2,...,l \tag{15}$$

where c_{2k} is the center vector, and b_{2k} is the base width.

The output layer neurons sum the product of the Gaussian vector calculated by the second hidden layer neuron and the weight, and serve as an output. The double-hidden-layer recurrent neural network output is expressed as:

$$Y = W \cdot H_2 = W_1 h_{21} + W_2 h_{22} + ... + W_l h_{2l} \tag{16}$$

In the controller (12), $f(x)$ is unknown part in practical application, DHLRNN can be employed to approximate $f(x)$. The block diagram of DHLRNN fractional sliding mode controller is shown in Fig.3.

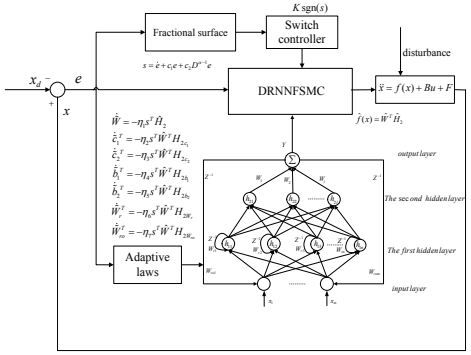

Fig.3. Block diagram of double-hidden-layer recurrent neural network fractional-order sliding mode controller

We suppose that there is an optimal weight W^*, optimal center c_1^* and c_2^*, optimal base width b_1^* and b_2^*, and optimal feedback weight W_r^* and W_{ro}^*,which can estimate the unknown function $f(x)$ expressed as $f(x) = W^{*T} H_2^* + \varepsilon$, where $H_2^* = H_2^*(x, c_1^*, c_2^*, b_1^*, b_2^*, W_r^*, W_{ro}^*)$, and ε is a small positive constant. We define $\hat{f}(x)$ as an estimate of $f(x)$ using a double-hidden-layer recurrent neural network. Then the difference between the unknown function $f(x)$ and its estimated value $\hat{f}(x)$ is:

$$\begin{aligned} f(x) - \hat{f}(x) &= W^{*T} H_2^* - \hat{W}^T \hat{H}_2 + \varepsilon \\ &= W^{*T} \hat{H}_2 + W^{*T} \tilde{H}_2 - \hat{W}^T \hat{H}_2 + \varepsilon \\ &= W^{*T} \hat{H}_2 - \hat{W}^T \hat{H}_2 + \hat{W}^T \tilde{H}_2 + \tilde{W}^T \tilde{H}_2 + \varepsilon \\ &= \tilde{W}^T \hat{H}_2 + \hat{W}^T \tilde{H}_2 + \tilde{W}^T \tilde{H}_2 + \varepsilon \\ &= \tilde{W}^T \hat{H}_2 + \hat{W}^T \tilde{H}_2 + \varepsilon_0 \end{aligned} \tag{17}$$

Calculate the Taylor expansion of $\tilde{H}_2$,

$$\begin{aligned} \tilde{H}_2 &= \frac{\partial H_2}{\partial c_1}\Big|_{c_1 = \hat{c}_1} (c_1^* - \hat{c}_1) + \frac{\partial H_2}{\partial c_2}\Big|_{c_2 = \hat{c}_2} (c_2^* - \hat{c}_2) \\ &+ \frac{\partial H_2}{\partial b_1}\Big|_{b_1 = \hat{b}_1} (b_1^* - \hat{b}_1) + \frac{\partial H_2}{\partial b_2}\Big|_{b_2 = \hat{b}_2} (b_2^* - \hat{b}_2) + \\ &\frac{\partial H_2}{\partial W_r}\Big|_{W_r = \hat{W}_r} (W_r^* - \hat{W}_r) + \frac{\partial H_2}{\partial W_{ro}}\Big|_{W_{ro} = \hat{W}_{ro}} (W_{ro}^* - \hat{W}_{ro}) + O_h \\ &= DH_{2c_1} \cdot \tilde{c}_1 + DH_{2c_2} \cdot \tilde{c}_2 + DH_{2b_1} \cdot \tilde{b}_1 \\ &+ DH_{2b_2} \cdot \tilde{b}_2 + DH_{2W_r} \cdot \tilde{W}_r + DH_{2W_{ro}} \cdot \tilde{W}_{ro} + O_h \end{aligned} \tag{18}$$

where O_h is a high-order term.

Replace unknown function $f(x)$ with $\hat{f}(x)$, then control law (12) is redesigned as:

$$u = -\frac{1}{b}(\hat{f}(x) - \ddot{x}_d + c_1\dot{e} + c_2 D^{\alpha} e) - K\,\mathrm{sgn}(s) \tag{19}$$

Select the Lyapunov function candidate as:

$$V=\frac{1}{2}s^Ts+\frac{1}{2\eta_1}tr(\tilde{W}^T\tilde{W})+\frac{1}{2\eta_2}tr(\tilde{c}_1^T\tilde{c}_1)+\frac{1}{2\eta_3}tr(\tilde{c}_2^T\tilde{c}_2)$$
$$+\frac{1}{2\eta_4}tr(\tilde{b}_1^T\tilde{b}_1)+\frac{1}{2\eta_5}tr(\tilde{b}_2^T\tilde{b}_2)+\frac{1}{2\eta_6}tr(\tilde{W}_r^T\tilde{W}_r)+\frac{1}{2\eta_7}tr(\tilde{W}_{ro}^T\tilde{W}_{ro}) \tag{20}$$

The last seven items are marked as $tr(*)$.

Differentiating equation (20), then we can get

$$\begin{aligned}\dot{V}&=s^T\dot{s}+tr(\dot{*})\\&=s^T[f(x)+bu+F-\ddot{x}_d+c_1\dot{e}+c_2D^\alpha e]+tr(\dot{*})\end{aligned} \tag{21}$$

Substituting the control law (19) into (21) yields,

$$\begin{aligned}\dot{V}&=s^T\left[f(x)-\hat{f}(x)+F-k\,\mathrm{sgn}(s)\right]+tr(\dot{*})\\&=s^T\left[\tilde{W}^T\hat{H}_2+\hat{W}^T\tilde{H}_2+\varepsilon_0+F-k\,\mathrm{sgn}(s)\right]+tr(\dot{*})\end{aligned} \tag{22}$$

Substituting the Taylor expansion (18) into equation (22), yields,

$$\begin{aligned}&\dot{V}=s^T\tilde{W}^T\hat{H}_2+s^T\hat{W}^T(DH_{2c_1}\cdot\tilde{c}_1+DH_{2c_2}\cdot\tilde{c}_2)\\&+s^T\hat{W}^T(DH_{2b_1}\cdot\tilde{b}_1+DH_{2b_2}\cdot\tilde{b}_2+DH_{2W_r}\cdot\tilde{W}_r+DH_{2W_{ro}}\cdot\tilde{W}_{ro}+O_h)\\&+s^T[\varepsilon_0+F-k\,\mathrm{sgn}(s)]+\frac{1}{\eta_1}tr(\tilde{W}^T\dot{\tilde{W}})+\frac{1}{\eta_2}tr(\dot{\tilde{c}}_1^T\tilde{c}_1)+\frac{1}{\eta_3}tr(\dot{\tilde{c}}_2^T\tilde{c}_2)\\&+\frac{1}{\eta_4}tr(\dot{\tilde{b}}_1^T\tilde{b}_1)+\frac{1}{\eta_5}tr(\dot{\tilde{b}}_2^T\tilde{b}_2)+\frac{1}{\eta_6}tr(\dot{\tilde{W}}_r^T\tilde{W}_r)+\frac{1}{\eta_7}tr(\dot{\tilde{W}}_{ro}^T\tilde{W}_{ro})\end{aligned} \tag{23}$$

Setting the adaptive laws as:

$$\begin{cases}\dot{\tilde{W}}=-\eta_1s^T\hat{H}_2,\dot{\tilde{c}}_1^T=-\eta_2s^T\hat{W}^TDH_{2c_1}\\\dot{\tilde{c}}_2^T=-\eta_3s^T\hat{W}^TDH_{2c_2},\dot{\tilde{b}}_1^T=-\eta_4s^T\hat{W}^TDH_{2b_1}\\\dot{\tilde{b}}_2^T=-\eta_5s^T\hat{W}^TDH_{2b_2},\dot{\tilde{W}}_r^T=-\eta_6s^T\hat{W}^TDH_{2W_r}\\\dot{\tilde{W}}_{ro}^T=-\eta_7s^T\hat{W}^TDH_{2W_{ro}}\end{cases} \tag{24}$$

Substituting adaptive laws (24) into (23), then we can get

$$\begin{aligned}\dot{V}&=s^T[\mathrm{F}+\varepsilon_0+O_h-K\,\mathrm{sgn}(S)]\\&\le|s|(H+\varepsilon_0+O_h-K)\end{aligned} \tag{25}$$

Assume that ε_0 and O_h exist upper bounds ε_E and O_E. If we make that $K\ge H+\varepsilon_E+O_E$, then we can guarantee that $\dot{V}\le 0$. $\dot{V}$ is semi-negative which ensures that both V and s are bounded. $\dot{V}\le|s|(H+\varepsilon_0+O_h-K)$ indicates that $\int_0^t|s|dt\le\frac{1}{H+\varepsilon_0+O_h-K}[V(t)-V(0)]$. Since $V(0)$ is bounded and $0\le V(t)\le V(0)$, $\lim_{t\to\infty}\int_0^t|s^T|dt$ is bounded. According to Barbalat's lemma $\lim_{t\to\infty}s=0$, that is, e and $\dot{e}$ converge to zero asymptotically..

5. HARDWARE EXPERIMENT VERIFICATION

In this paper, a hardware experiment is implemented to verify the effectiveness of the DHLRNNFSMC scheme using dSPACE 1104 real-time system. The overall structure of the single-phase APF is shown in Fig.4. The experimental prototype is shown in Fig.5.

We use programmable AC source as the single-phase grid power where the frequency and the voltage are 50HZ and 24V, respectively. The main circuit of APF is a single-phase shunt active power filter, selecting IGBT as the main circuit switching device. The signal collection circuit adopts Hall voltage sensors CHV-25P and Hall current sensors CSM002A to collect voltage signals and current signals. The dSPACE control circuit is based on dSPACE 1104, which is connected to APF through ADC and PWM output ports. The signals collected by the signal collection circuit are sent to the ADC and calculated by dSPACE. Then the signals are sent out to the IGBT driver by PWM output ports. The nonlinear loads are composed of a single phase uncontrolled rectifier bridge and a capacitive load. In addition, the IGBT drive circuit and the signal collection circuit are powered by a DC auxiliary power source. The current spectrum analysis was performed using the DSOX3PWR power measurement application and analysis module of the Agilent DSO-X3034A oscilloscope. In the experiment, the parameters are list in Table 1.

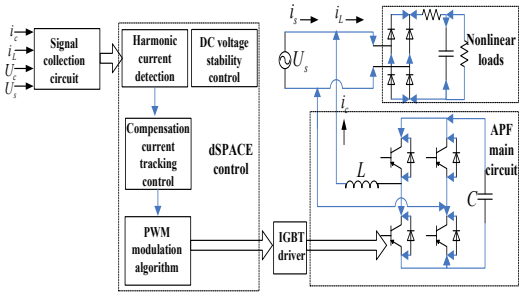

Fig.4. The overall structure of the single-phase APF

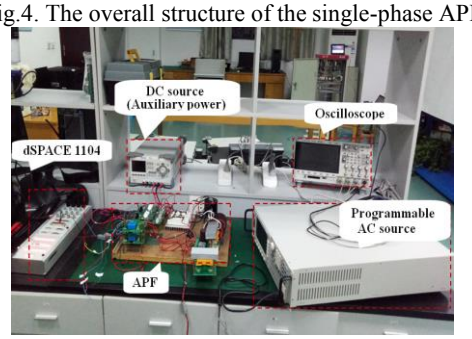

Fig.5. Single-phase APF experimental setup system

Table 1. System experimental parameters

System parameters	Nominal value
Supply voltage and frequency	$V_s=220V, f=50Hz$
Single-phase diode rectifiers parameters	$R_1=15\Omega, C_1=1mF$
Active power filter parameters	$L=10mH, R=0.1\Omega$ $C=2200\mu F, v_{dcref}=50V$
Switching frequency	$f_{sw}=20KHz$

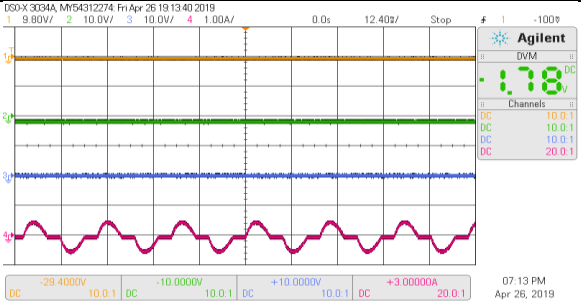

(a) Supply current without APF

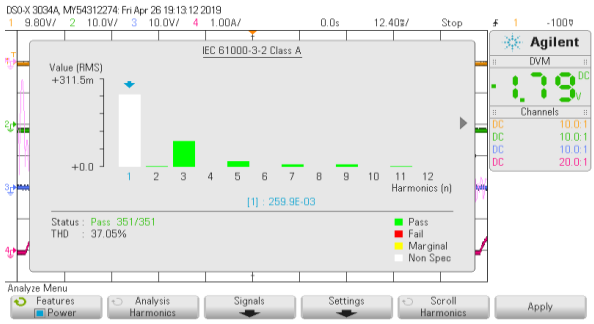

(b) THD of supply current without APF

Fig.6 Power supply current analysis without APF

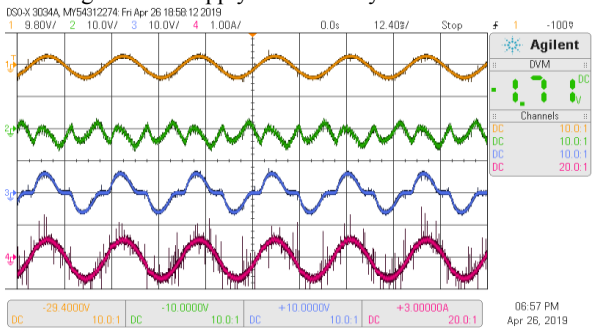

(a) Steady state response of DRNNFSMC scheme

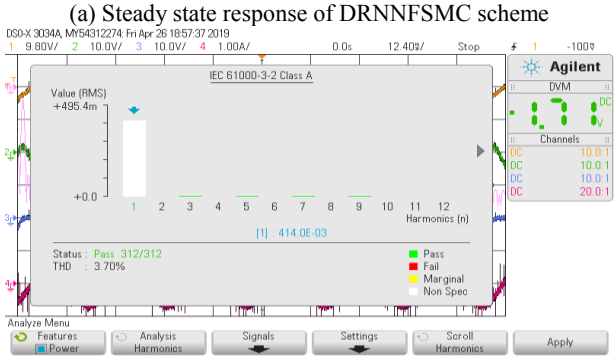

(b) THD of DHLRNNFSMC scheme

Fig.7. Steady-state experiment of DRNNFSMC scheme

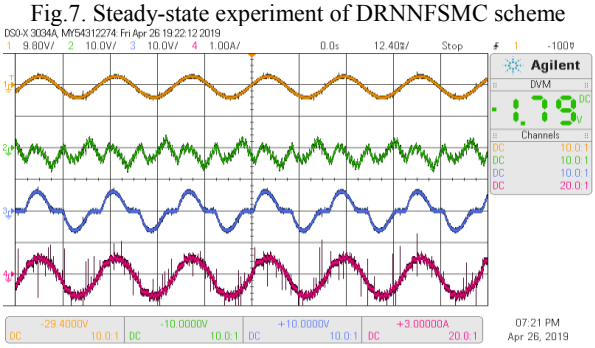

(a) Steady state response of NNSMC scheme

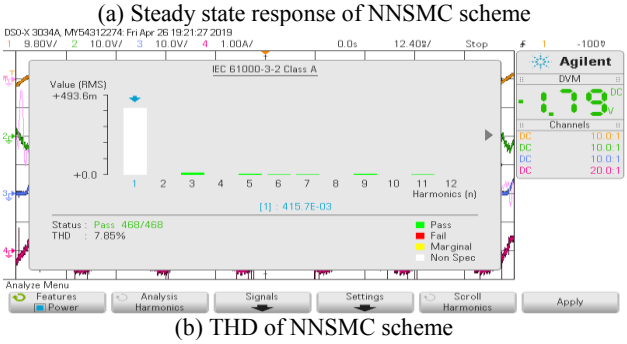

(b) THD of NNSMC scheme

Fig.8. Steady-state experiment of NNSMC scheme

A. Steady state response and comparative study

The proposed DHLRNNFSMC method and the common neural network sliding mode control method (NNSMC) are applied to the APF, respectively. Fig.6 (a) is a waveform curve of the supply current i_s before the APF is accessed, and Fig.6 (b) is a corresponding spectrum analysis diagram. Fig.7 (a) and Fig.8 (a) are steady-state response waveform diagrams using the DHLRNNFSMC and NNSMC control method, respectively. The waveforms are the power supply voltage v_s, the compensation current i_c, the load current i_L, and the power supply current i_s, respectively. Fig.7 (b) and Fig.8 (b) are corresponding spectrum analysis diagrams. THD of the power supply current is reduced from 37.05% to 3.7% with the connection of APF, and the power supply current is approximately compensated as a sine wave, realizing the purpose of current compensation. Compared with the NNSMC method, the proposed DHLRNNFSMC scheme has smaller glitch and chattering, smaller THD, better robustness and higher compensation accuracy.

B. Dynamic response

The dynamic performance of the proposed scheme is verified by increasing load and decreasing load suddenly. Fig.9 and Fig.10 show the system response process during load burst and load dump. Fig.9 (a) and Fig.9 (b) are the waveform diagram of the system response and the spectrum analysis diagram of the power supply current during the load sudden increasing. Fig.10 (a) and Fig.10 (b) are the cases during the load sudden decreasing. The power supply current can enter a new stable state quickly regardless of the sudden increase or decrease of the load, showing the proposed algorithm has good adaptability to load disturbance.

Fig.8. Steady-state experiment of NNSMC schem

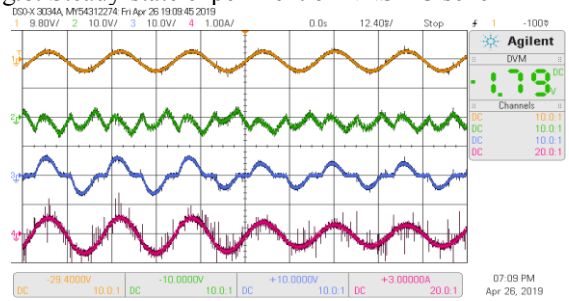

(a) Dynamic response of loads increase

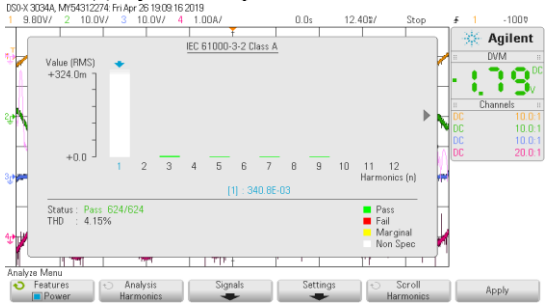

(b) Spectrum analysis of loads increase

Fig.9. Dynamic experiment of loads increase

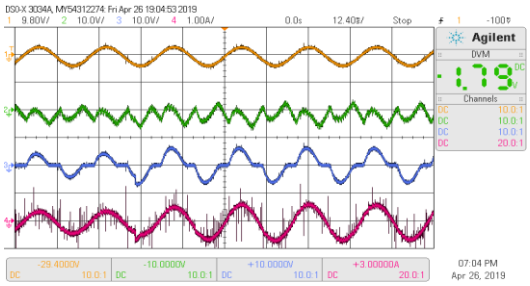

(a) Dynamic response of loads decrease

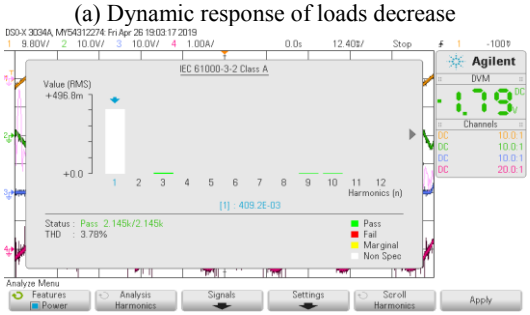

(b) Spectrum analysis of loads decrease

Fig.10. Dynamic experiment of loads decrease

6. CONCLUSION

In this paper, a fractional-order sliding mode controller based on a double-hidden-layer recurrent neural network is designed to compensate grid harmonic current. A double-hidden-layer recurrent neural network is designed to approximate the unknown nonlinear part of APF. The base width, center vector and weight in the network have self-adjusting performance. Fractional sliding mode controller combines the advantages of fractional calculus and sliding mode control, improving the control precision and performance. The experimental verification are realized on dSPACE 1104, showing the proposed DHLRNNFSMC scheme can quickly compensate the power supply current with better current tracking effect, indicating the superiority and effectiveness of the proposed scheme.

ACKLOWLEDGEMENT

This work is partially supported by National Science Foundation of China under Grant No. 61873085; Natural Science Foundation of Jiangsu Province under Grant No. BK20171198.

REFERENCES

Chen, G., Song, Y. and Guan, Y. (2018). Terminal Sliding Mode-Based Consensus Tracking Control for Networked Uncertain Mechanical Systems on Digraphs, *IEEE Trans on Neural Networks and Learning Systems*, 29(3), pp. 749-756.

Chu, Y., Fei, J. and Hou, S. (2019). Adaptive Global Sliding-Mode Control for Dynamic Systems Using Double-hidden-layer recurrent Neural Network Structure, *IEEE Trans on Neural Network and Learning Systems*. DOI:10.1109/TNNLS. 2019.2919676.

Fan, Q. and Yang, G. (2016). Adaptive Actor-Critic Design-Based Integral Sliding-Mode Control for Partially Unknown Nonlinear Systems With Input Disturbances, *IEEE Trans on Neural Networks and Learning Systems*, 27(1), pp.165-177.

Fei, J. and Wang, T. (2019). Adaptive fuzzy-neural-network based on RBFNN control for active power filter, *International Journal of Machine Learning and Cybernetics*, 10(5), pp. 1139-1150.

Fang, Y., Fei, J. and Cao, D. (2019). Adaptive Fuzzy-Neural Fractional-Order Current Control of Active Power Filter with Finite-Time Sliding Controller, *International Journal of Fuzzy System*, 21(5), pp.1533-1543.

Hao, L., Park, J. and Ye, D. (2017). Integral Sliding Mode Fault-Tolerant Control for Uncertain Linear Systems Over Networks With Signals Quantization, *IEEE Trans on Neural Networks and Learning Systems*, 28(9), pp. 2088-2100.

Ionescu, C. and Muresan, C. (2015). Sliding Mode Control for a Class of Sub-Systems with Fractional Order Varying Trajectory Dynamics, *Fractional Calculus and Applied Analysis*, 18(6), pp. 1441-1451.

Liu, D. and Yang, G. (2019). Prescribed Performance Model-Free Adaptive Integral Sliding Mode Control for Discrete-Time Nonlinear Systems, *IEEE Trans on Neural Networks and Learning Systems*, 30(7), pp. 2222-2230.

Park, J., Kim, S. and Park, T. (2019). Output-Feedback Adaptive Neural Controller for Uncertain Pure-Feedback Nonlinear Systems Using a High-Order Sliding Mode Observer, *IEEE Trans on Neural Networks and Learning Systems*, 30(5), pp. 1596-1601.

Song, S., Zhang, B. and Song, X. (2019). Fractional-order Adaptive Neuro-fuzzy Sliding Mode H-infinity Control for Fuzzy Singularly Perturbed Systems, *Journal of the Franklin Institute-Engineering and Applied Mathematics*, 356(10), pp. 5027-5048.

Tuan, L. (2019). Fractional-order Fast Terminal Back-stepping Sliding Mode Control of Crawler Cranes, *Mechanism and Machine Theory*, 137, pp. 297-314.

Wang, H. and Fei, J. (2019). Nonsingular Terminal Sliding Mode Control for Active Power Filter Using Recurrent Neural Network, *IEEE Access*, 6, pp. 67819-67829.